CrossMark

High-Temperature Tensile Strength of $Al_{10}Co_{25}Cr_8Fe_{15}Ni_{36}Ti_6$ Compositionally Complex Alloy (High-Entropy Alloy)

H.M. DAOUD,[1] A.M. MANZONI,[2] N. WANDERKA,[2] and U. GLATZEL[1,3]

1.—Metals and Alloys, Bayreuth University, 95447 Bayreuth, Germany. 2.—Helmholtz-Zentrum Berlin für Materialien und Energie GmbH, 14109 Berlin, Germany. 3.—e-mail: uwe.glatzel@uni-bayreuth.de

Homogenizing at 1220°C for 20 h and subsequent aging at 900°C for 5 h and 50 h of a novel $Al_{10}Co_{25}Cr_8Fe_{15}Ni_{36}Ti_6$ compositionally complex alloy (high-entropy alloy) produces a microstructure consisting of an $L1_2$ ordered γ' phase embedded in a face-centered cubic solid-solution γ matrix together with needle-like B2 precipitates (NiAl). The volume fraction of γ' phase is ~46% and of needle-like B2 precipitates <5%, which is in accordance with the prediction of calculation of phase diagram method (CALPHAD using Thermo-Calc software with TTNi7 database; Thermo-Calc Software, Stockholm, Sweden). The high-temperature tensile tests were carried out at room temperature, 600°C, 700°C, 800°C, and 1000°C. The tensile strength as well as the elongation to failure of both heat-treated specimens is very high at all tested temperatures. The values of tensile strength has been compared with literature data of well-known Alloy 800H and Inconel 617, and is discussed in terms of the observed microstructure.

INTRODUCTION

Compositionally complex alloys, originally named high-entropy alloys,[1,2] have been intensively investigated since their discovery at the turn of the century. It has been supposed that the high mixing entropy of at least five alloying elements would enhance the formation of a single solid solution.[1,2] However, after one decade of investigation of these alloys, only few of them have been found consisting of a single solid solution.[3–9] The compositionally complex alloys (high-entropy alloys) can be classified mainly into two groups according to whether the main phase is either face-centered cubic (fcc)[3,7] or body-centered cubic (bcc).[8,9] The first can be tested under a tensile load, but their strength values are small.[7,10] The latter show high compressive strength up to 1000°C,[8,9] but because of their brittleness, these alloys cannot be tested in tension. However, a new high entropy alloy with hexagonal close-packed (hcp) solid solution has been recently published.[4]

Our main goal is to optimize the compositionally complex alloys (high-entropy alloys) to be used in high-temperature applications above 600°C. The first step is to optimize the microstructure of the candidate alloys to enhance the strength at elevated temperatures. Across time, the two-phase morphology has been found most promising, namely a fcc matrix containing precipitates with an ordered $L1_2$ structure, as it is the case in many Ni-based superalloys. Ordered γ' precipitates have a great effect onto increasing both the yield and the ultimate strength with increasing temperature. This strengthening effect is explained by precipitate hardening, the temperature anomalous behavior of $L1_2$ precipitates, and coherency stresses.[11,12]

From our previous work,[10] we identified the alloy $Al_8Co_{17}Cr_{17}Cu_8Fe_{17}Ni_{33}$ (in the following named "initial fcc alloy") to be promising because of the following properties: Its microstructure consists of a matrix with fcc structure containing about 20 vol.% of γ' precipitates with an ordered $L1_2$ structure and with a diameter smaller than 20 nm; it shows high elongation to failure under tensile load; and it exhibits very good oxidation resistance up to 1000°C in air.[13] The challenge now is to enhance its low strength by increasing the size and volume fraction of the γ' precipitates.

Therefore, changes of the equilibrium phase diagram by the addition of elements like Mn, Ti, Mo, Re, and W have been investigated using the

calculation of phase diagram (CALPHAD) method. In Ni-based superalloys, it is well known that the use of specific elements has a great effect on the volume fraction of both the $L1_2$ ordered γ' phase and the fcc γ matrix. The four alloying elements (Al, Ti, Co, and Ni) stabilize the γ' precipitates.[12] This knowledge has been adapted to our alloys and thus compositional changes of these four elements have been carefully adjusted because the increase of Al and/or Ti increases the possibility of the formation of brittle phases, as has been reported in other compositionally complex alloys (high-entropy alloys).[14] At the same time, the increase of Ni and Co is restricted according to our self-imposed rule (and one of the extended definitions of high-entropy alloys): no element is allowed to exceed 35 at.%.[1,2] Additionally, Cu has been completely eliminated in the new optimized alloy to inhibit the formation of a Cu rich fcc phase, which was observed in the previously studied "initial fcc alloy" $Al_8Co_{17}Cr_{17}Cu_8Fe_{17}Ni_{33}$.[10] Finally, the Cr content has been reduced to eliminate the formation of brittle σ phases, leading to a brittle alloy.[10,13]

Thus, a new "optimized fcc alloy" with the composition $Al_{10}Co_{25}Cr_8Fe_{15}Ni_{36}Ti_6$ (at.%) has been selected by CALPHAD calculations (Thermo-Calc with TTNi7 database[15,16]) of 190 different alloys. In this work, we present the mechanical properties of the optimized alloy $Al_{10}Co_{25}Cr_8Fe_{15}Ni_{36}Ti_6$ under a tensile load at different temperatures.

EXPERIMENTAL

The investigated $Al_{10}Co_{25}Cr_8Fe_{15}Ni_{36}Ti_6$ (at.%) alloy was produced from constituent elements of 99.99%. It was casted in a vacuum induction furnace and poured into ceramic molds with a length of 140 mm and with a diameter of 10 mm. Samples were solidified directionally with preferred $\langle 001 \rangle$ direction using the Bridgman method. Ceramic shell molds known from single-crystal wax-lost precision casting have been used. The as-cast alloy was homogenized at 1220°C for 20 h, cooled in the furnace, and subsequently aged at 900°C for 5 h and 50 h. The aging was followed by cooling in air. Tensile tests on the aged alloy were carried out at room temperature (RT), 600°C, 700°C, 800°C, and 1000°C using a universal testing machine (Z100/TL35; Zwick USA, Kennesaw, GA) at a displacement rate of 5 mm/min. Cylindrical tensile specimens with a gauge length of 25 mm and a diameter of 5 mm have been prepared according to DIN 50 125.[17] The equilibrium phase diagram of the investigated alloy was calculated using Thermo-Calc software[15] and TTNi7 database.[16] The TTNi7 database is used for Ni-based superalloys and according to our previous work,[3,10] the use of this database on a high-entropy alloy system shows in certain compositional areas a good agreement with the experimental results. The microstructure of the alloy in all the tested states was characterized using of optical microscopy (Axioplan 2; Carl Zeiss, Oberkochen, Germany) and scanning electron microscopy (SEM; Zeiss 1540 EsB CrossBeam) equipped with an energy-dispersive x-ray spectrometer (EDX; Noran System Six; Thermo Fisher Scientific Inc., Waltham, MA) and transmission electron microscopy (TEM; Philips CM30; Philips, Amsterdam, the Netherlands) operated at 300 kV. The chemical composition of the phases has been analyzed by TEM/EDX with a beam size of 10 nm in diameter. The specimens for SEM were prepared using standard metallographic procedures and those for TEM using a method described in Ref 3. The volume fraction of the precipitates and its diameter were calculated using image analysis software (Stream view 1.4; Olympus Soft Imaging Solutions, Münster, Germany).

RESULTS

Equilibrium Phase Diagram of the $Al_{10}Co_{25}Cr_8Fe_{15}Ni_{36}Ti_6$ Alloy

The thermodynamic calculations of equilibrium phases in multicomponent alloys $Al_8Co_{17}Cr_{17}Cu_8Fe_{17}Ni_{33}$ and $Al_{10}Co_{25}Cr_8Fe_{15}Ni_{36}Ti_6$ are shown in Fig. 1a and b, respectively. The alloy of composition $Al_8Co_{17}Cr_{17}Cu_8Fe_{17}Ni_{33}$ has been widely investigated[3] and it has been used as a basis for a further optimization. According to the phase diagrams displayed in Fig. 1, the corresponding changes in composition of the $Al_8Co_{17}Cr_{17}Cu_8Fe_{17}Ni_{33}$ alloy increase the volume fraction of the γ' precipitates and enlarge the stability of the γ' phase up to 1100°C in the alloy $Al_{10}Co_{25}Cr_8Fe_{15}Ni_{36}Ti_6$. Moreover, the formation of the brittle phase sigma has been shifted to temperatures below 600°C and B2 (NiAl) volume fraction has been reduced. The predicted phases in the equilibrium phase diagram marked by bcc or bcc-2 could not be found in the investigated alloy and will therefore be ignored.

The calculated phase diagram in Fig. 1b indicates an annealing window of 1150°C to 1250°C, which was used for homogenization. The γ' phase starts to precipitate at 1150°C. According to the predicted phase diagram the volume fraction of the γ' precipitates increases rapidly and reaches about 50 vol.% at 900°C.

Microstructure of the $Al_{10}Co_{25}Cr_8Fe_{15}Ni_{36}Ti_6$ Alloy

The dendritic/interdendritic microstructure of the as-cast alloy is shown in Fig. 2 by SEM. The chemical composition of the dendritic (marked by 1) and interdendritic region (marked by 2), measured by SEM/EDX, is listed in Table I. The dendrites as well as the interdendritic region consist of precipitates. Due to the small sizes of the γ' precipitates it is difficult to measure their composition using SEM/EDX. However, the measured average amount of Co and Cr is higher in the dendrites, whereas the
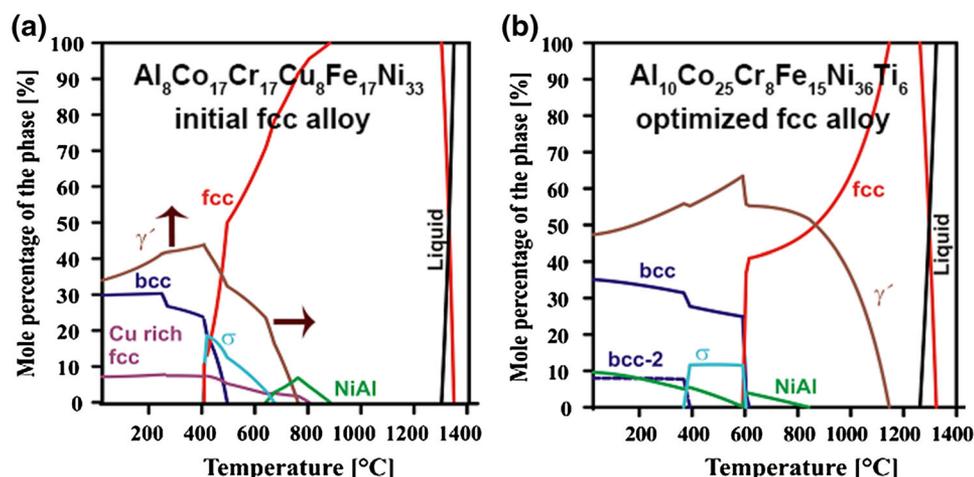
Fig. 1. Calculated phase diagrams of (a) "initial fcc alloy" and (b) "optimized fcc alloy"; using of Thermo-Calc software[15] with TTNi7 database.[16] The readers are recommended to refer to the online version of the article, because this figure is illustrated in color.

interdendritic regions are significantly enriched in Ti.

After the homogenization at 1220°C for 20 h and the subsequent heat treatment at 900°C, the specimens are characterized by a three-phase morphology: up to 50-μm-long needle-shape precipitates of NiAl type, γ' precipitates of Ni_3Al type, about 450 nm in diameter and the fcc matrix. In the following, the NiAl needles are being disregarded because of their small volume fraction (<5 vol.%). The chemical compositions of the γ' precipitates and the matrix after the heat treatments at 900°C are also listed in Table I. These measurements were carried out by TEM/EDX.

Intensive experimental work has been carried out to find the right temperature and the time to homogenization and aging temperature (between 800°C and 1000°C) to optimize the microstructure. According to Fig. 1b, at temperatures higher than 1000°C, the γ' precipitates will dissolve. At temperatures below 800°C, there is the possibility to form and to stabilize brittle phases like sigma and NiAl. The optimized homogenization temperature and the time have been found experimentally to be 1220°C and 20 h. The subsequent aging temperature at 900°C has been chosen according to the calculated phase diagram (see Fig. 1b), and it was experimentally found to be the best to produce fairly large γ' precipitates and to push their volume fraction to a maximum. For a comparison of the alloy's microstructure and its mechanical properties, it has been decided to age the alloy for 5 h and 50 h. The resulting microstructures are shown in Fig. 3.

The SEM micrographs (Fig. 3) illustrate the microstructure of the alloy after homogenization and subsequent aging at 900°C for 5 h and for 50 h. No precipitates are visible in Fig. 3a. A two-phase microstructure, as shown in Fig. 3b and c, is obtained after aging. In the specimen aged at 900°C for 5 h, the γ' precipitates have a volume fraction of approximately 45 vol.% and a diameter of 450 ± 120 nm. In the specimen aged at 900°C for 50 h, they have 46 vol.% and a diameter of 460 ± 100 nm.

TEM investigations of the aged samples (not shown here) show very small secondary $Ni_3(Al,Ti)$ γ' precipitates of about 10 nm in size in the matrix of the specimen aged for 5 h. These precipitates are not present in the specimen aged for 50 h.

Mechanical Properties of the $Al_{10}Co_{25}Cr_8Fe_{15}Ni_{36}Ti_6$ Alloy

Figure 4a and b shows the tensile stress–strain curves of the differently aged specimens. The detailed results of the yield strength (σ_Y), ultimate tensile strength (σ_{TS}), uniform strain (ε_{TS}), and elongation to failure (ε_f) are listed in Table II.

A similar tendency in mechanical behavior can be observed for samples aged for 5 h and 50 h aging time. The value of the yield strength and the ultimate tensile strength are the highest for samples tested at RT. However, the value of the yield strength at RT of the sample aged for 50 h is approximately 25% higher than that of the sample aged for 5 h. As expected, with increasing testing temperature, these values decrease. However, this trend at temperatures 600°C, 700°C, and 800°C is small and the values are close to each other. In the case of the sample aged at 900°C for 5 h, the average values of ultimate tensile strength is about 682 MPa and the yield strength about 508 MPa. A comparison with the samples aged at 900°C for 50 h shows that their average values of ultimate tensile strength and yield strength correspond to 707 MPa and 525 MPa, respectively, which are a little higher than those of the samples aged for 5 h. An exception has been observed for the sample (900°C for 5 h) tested at 1000°C, in which the yield strength decreases to 148 MPa.
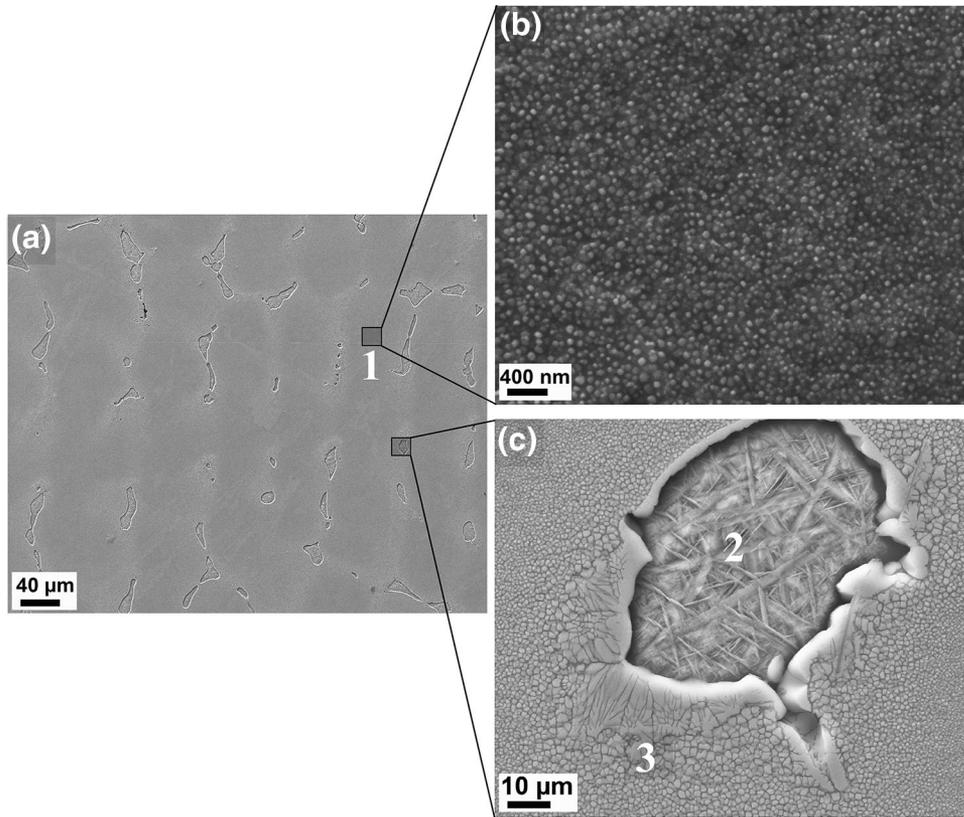
Fig. 2. SEM micrographs of the as-cast $Al_{10}Co_{25}Cr_8Fe_{15}Ni_{36}Ti_6$ alloy: (a) the dendritic and interdendritic regions at low magnification, (b) the precipitates in the dendritic region, and (c) the precipitates in the transition zone at high magnification.

Table I. The chemical composition (in at.%) of the $Al_{10}Co_{25}Cr_8Fe_{15}Ni_{36}Ti_6$ alloy in as-cast state measured by SEM/EDX

Phase/zone	Al	Co	Cr	Fe	Ni	Ti
As cast						
Dendrite—Zone 1	9.3	25.7	9.0	14.4	35.2	6.0
Interdendrite—Zone 2	12.8	20.8	4.1	8.2	37.4	16.6
Interdendrite—Zone 3	7.7	22.8	5.4	10.3	40.2	13.7
1220°C to 900°C, 5 h						
γ matrix	9.6 ± 2.0	28.1 ± 1.7	9.1 ± 0.8	18.6 ± 1.1	31.1 ± 1.3	3.5 ± 0.4
γ' precipitates	14.7 ± 1.0	21.5 ± 1.1	3.7 ± 0.5	8.1 ± 0.6	44.1 ± 1.2	7.9 ± 0.8
1220°C to 900°C, 50 h						
γ matrix	7.1 ± 0.7	29.6 ± 0.5	9.4 ± 0.2	20.5 ± 0.2	30.0 ± 0.4	3.5 ± 0.2
γ' precipitates	11.3 ± 0.2	22.9 ± 0.5	3.7 ± 0.4	9.0 ± 0.9	44.7 ± 1.6	8.5 ± 0.3

After heat treatment at 900°C, measured by TEM/EDX. The average standard deviation for SEM/EDX is ≤0.3 at.%. Zones 1–3 correspond to the areas marked in Fig. 2.

The observed values of elongation to failure and their corresponding uniform strains at all tested temperatures except at 800°C have similar values, even when comparing the aging times of 5 h and 50 h. However, at 800°C, the uniform strain is much smaller than its corresponding elongation to failure (see Table II). This observation in behavior is valid for both aged samples (at 5 h and 50 h). Extremely high elongation up to 92% has been observed for the sample tested at 1000°C. In the case of sample aged at 900°C for 5 h, the elongation increases with the increasing test temperature. Compared with the sample aged at 900°C for 50 h, first an increase of the elongation has been observed at 600°C but then a decrease with increasing temperature up to 800°C.

High-Temperature Tensile Strength of $Al_{10}Co_{25}Cr_8Fe_{15}Ni_{36}Ti_6$
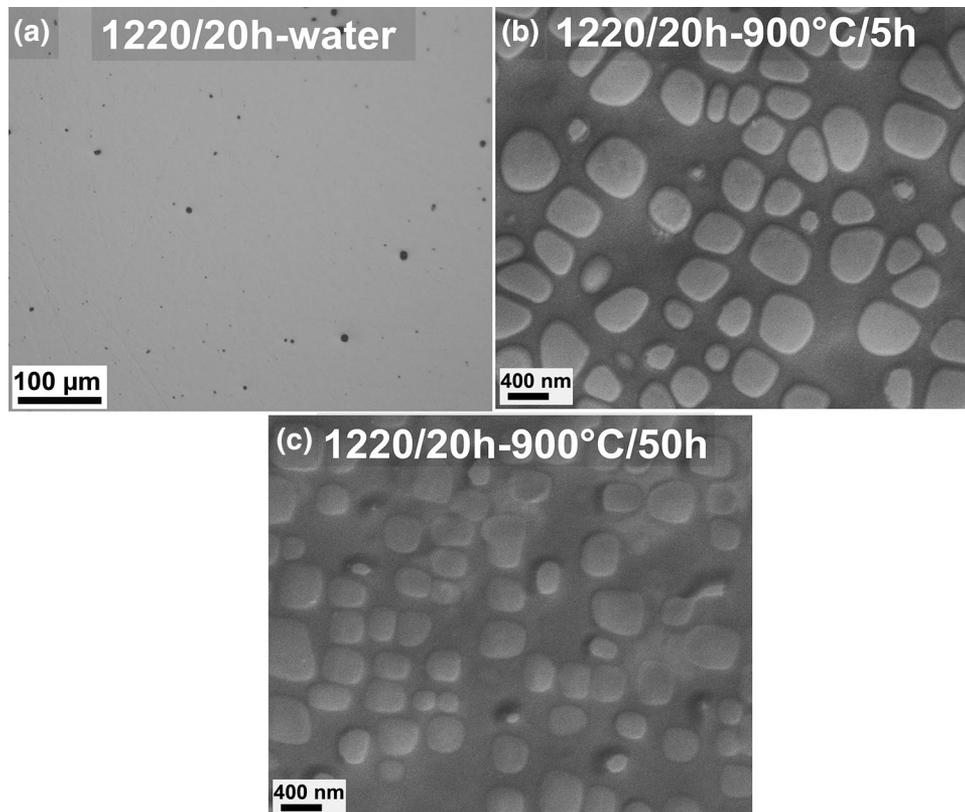Compositionally Complex Alloy (High-Entropy Alloy)

Fig. 3. (a) Optical micrograph of the homogenized specimen at 1220°C for 20 h. (b and c) SEM-micrographs of the specimens after homogenization at 1220°C for 20 h and followed by aging at 900°C for (b) 5 h and (c) for 50 h.
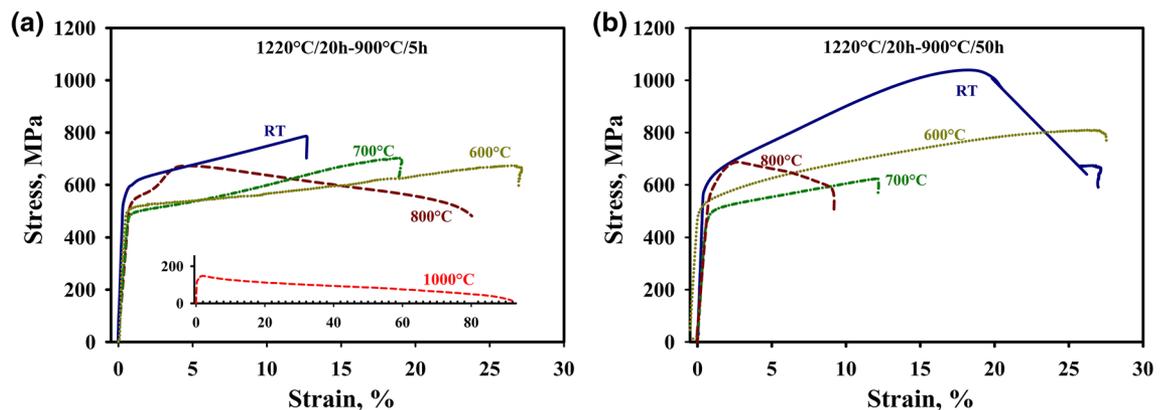

Fig. 4. Tensile stress–strain curves at RT, 600°C, 700°C, 800°C, and 1000°C of the heat-treated specimens at (a) 1220°C/20 h–900°C/5 h and (b) 1220°C/20 h–900°C/50 h.

DISCUSSION

Equilibrium Phase Diagram of $Al_{10}Co_{25}Cr_8$ $Fe_{15}Ni_{36}Ti_6$ Alloy

The formation of γ' precipitates in the disordered fcc matrix and their volume fraction (approximately 46%) observed in the $Al_{10}Co_{25}Cr_8Fe_{15}Ni_{36}Ti_6$ alloy (aged at 900°C) corresponds well to the prediction from the calculated equilibrium phase diagram (see Fig. 1b). The formation of NiAl precipitates as well as their volume fraction ($<5\%$) is also in good agreement. The CALPHAD method proves to be a powerful tool for the prediction of the $Al_{10}Co_{25}Cr_8$ $Fe_{15}Ni_{36}Ti_6$ compositionally complex alloy, as has been the case for $Al_8Co_{17}Cr_{17}Cu_8Fe_{17}Ni_{33}$ in previous works.[3,10]

Table II. Mechanical properties under tensile stress of the $Al_{10}Co_{25}Cr_8Fe_{15}Ni_{36}Ti_6$ alloy: the yield strength (σ_Y), ultimate tensile strength (σ_{TS}), uniform strain (ε_{TS}), and elongation to failure (ε_f)

T (°C)	σ_{TS} (MPa)	σ_Y (MPa)	ε_{TS} (%)	ε_f (%)
1220°C/20 h–900°C/5 h				
RT	786	568	12	12
600	674	501	26	26
700	702	487	18	18
800	672	535	4	27
1000	148	–	–	92
1220°C/20 h–900°C/50 h				
RT	1039	596	17	20
600	809	509	26	27
700	624	486	11	11
800	687	581	2	9

Microstructure of the $Al_{10}Co_{25}Cr_8Fe_{15}Ni_{36}Ti_6$ Alloy

Previously investigated alloys show in their microstructure the formation of only small amounts of small precipitate sizes of γ' phase; e.g., the as-cast alloy with composition of $Al_9Co_{18}Cr_{18}Cu_{18}Fe_{18}Ni_{19}$ contains a small amount of γ' precipitates with size of 5–10 nm, where the volume fraction of those precipitates were not written in the corresponding literature.[18] The alloy $Al_8Co_{17}Cr_{17}Cu_8Fe_{17}Ni_{33}$ in both as-cast and heat treated at 700°C for 5 h specimens contains less than 20% of γ' precipitates with diameters smaller than 20 nm.[10] The novel $Al_{10}Co_{25}Cr_8Fe_{15}Ni_{36}Ti_6$ alloy shows a high volume fraction of γ' phase (~46%) and a size of approximately 450 nm of the γ' precipitates that, to our knowledge, have not been reported in compositionally complex alloys before.

The size of the γ' precipitates in the $Al_{10}Co_{25}Cr_8Fe_{15}Ni_{36}Ti_6$ is practically the same after 5 h and 50 h aging at 900°C within the material scatter. This size is close to 500 nm, which has been found as the optimum size regarding mechanical properties in Ni-based superalloys.[12] The secondary γ' precipitates that are visible after aging during 5 h disappear after the longer aging time of 50 h, which results in a slightly larger size and thus a slight coarsening of the primary γ' precipitates after 50 h. In single-crystal Ni-based superalloys, a maximum creep life at high temperatures (> 900°C) is achieved with a microstructure containing 70 ± 10 vol.% of γ' precipitates. The Ni-base superalloys optimized for temperatures around 700°C have in general γ' volume fractions < 50%. This is an indicator that our "optimized fcc alloy" $Al_{10}Co_{25}Cr_8Fe_{15}Ni_{36}Ti_6$ can be used in similar creep-related applications in a temperature regime of 600°C to 800°C.

Comparison of Mechanical Properties of the "Optimized fcc Alloy" $Al_{10}Co_{25}Cr_8Fe_{15}Ni_{36}Ti_6$ Alloy with Commercially Available Alloys

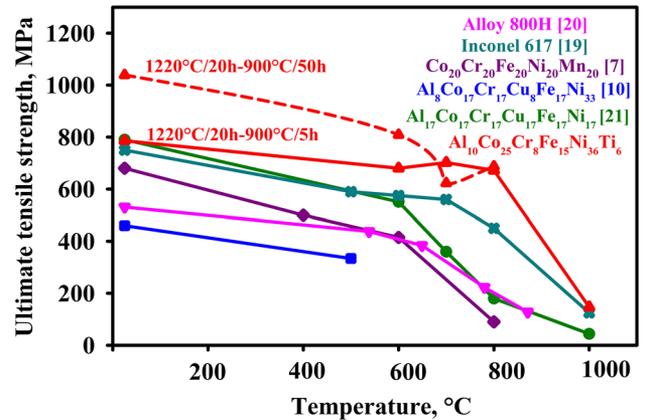Figure 5 shows a comparison of the tensile strength as a function of temperature between both

Fig. 5. Comparison of the tensile strength as a function of temperature between the novel $Al_{10}Co_{25}Cr_8Fe_{15}Ni_{36}Ti_6$ alloy in heat-treated conditions and commercial alloys Inconel 617,[19] Alloy 800H,[20] fcc solid solution forming alloys ["initial fcc alloy" (Ref. 10) and $Co_{20}Cr_{20}Fe_{20}Ni_{20}Mn_{20}$ (Ref. 7)] and the most investigated compositionally complex alloy $Al_{17}Co_{17}Cr_{17}Cu_{17}Fe_{17}Ni_{17}$ (Ref. 21).

heat-treated states of the $Al_{10}Co_{25}Cr_8Fe_{15}Ni_{36}Ti_6$ alloy and several other commercially available.[19,20] The decrease in strength of the $Al_{10}Co_{25}Cr_8Fe_{15}Ni_{36}Ti_6$ alloy with increasing temperature is small up to 800°C, especially for the sample annealed only for 5 h at 900°C. The resulting good stability of this annealed alloy can probably be attributed to the high volume fraction and optimal size of the γ' precipitates embedded in the γ matrix. This precipitate strengthening effect is mainly a result of three hardening mechanisms. One is due to the small difference between lattice parameters of the γ' phase and the matrix phase (coherency stress). The other is due to the high energy that is required on the one hand to build antiphase boundaries and on the other hand to move dislocations in a ordered morphology.[11,12] For optimized volume fractions and γ' size, Orowan bowing of dislocation leads to an additional strengthening term. The high tensile strength of the "optimized fcc alloy" $Al_{10}Co_{25}Cr_8Fe_{15}Ni_{36}Ti_6$ can be attributed to these three hardening mechanisms.

The strength decreases very rapidly at 1000°C for the specimen aged for 5 h at 900°C down to 148 MPa, combined with a very high elongation to failure of 92% (see Table II). According to the equilibrium phase diagram (Fig. 1b), the γ' precipitates dissolve rapidly above 950°C with increasing temperatures until total disappearance at 1150°C. This results in the rapid strength loss.

The tensile strength of the specimen aged for 50 h at 900°C is in general higher than the tensile strength of the 5 h aged specimen. The coarsening of the primary γ' precipitates along with compositional and misfit is the cause for this.

Compared with commercial alloys Inconel 617[19] and Alloy 800H[20] and with two fcc solid-solution-forming high-entropy alloys ["initial fcc alloy" $Al_8Co_{17}Cr_{17}Cu_8Fe_{17}Ni_{33}$ (Ref. 10) and $Co_{20}Cr_{20}Fe_{20}Ni_{20}Mn_{20}$ (Ref. 7)] and the most intensively investigated compositionally complex alloy $Al_{17}Co_{17}Cr_{17}Cu_{17}Fe_{17}Ni_{17}$ (Ref. 21), our "optimized fcc alloy" $Al_{10}Co_{25}Cr_8Fe_{15}Ni_{36}Ti_6$ shows higher tensile strength at all temperatures. Inconel 617 shows the same qualitative behavior as the investigated alloy. Its strength can be attributed to carbide formation and γ' precipitates.[19] The density of our "optimized fcc alloy" is approximately 5% lower than that of Inconel 617, whereas the cost, by just calculating the alloying elements, is by a factor of 1.6 higher. The alloy ($Al_{17}Co_{17}Cr_{17}Cu_{17}Fe_{17}Ni_{17}$) shows high strength at low temperatures due to the presence of a bcc phase and a dramatic loss in strength above 600°C due to the transition from brittle to ductile mechanical response.[21]

CONCLUSION

In this work, a novel $Al_{10}Co_{25}Cr_8Fe_{15}Ni_{36}Ti_6$ compositionally complex alloy (high-entropy alloy) has been chosen from 190 other possible alloys and has been investigated by scanning electron microscopy, transmission electron microscopy, and high-temperature tensile testing. The microstructure of this alloy after homogenization at 1220°C and subsequent heat treatment at 900°C for 5 h or 50 h consists of a fcc matrix, γ' precipitates with approximately 46 vol.% and an average size of about 450 nm. In addition, secondary γ' precipitates have been observed and less than 5% of up to 50 μm long needle-like NiAl precipitates after 5 h aging time. As a result of optimized γ' volume fraction and size,

this alloy shows high-temperature tensile strength up to 800°C, accompanied by a high elongation to failure. The strength decreases only slightly at 800°C and falls off at approximately 1000°C. At all tested temperatures the tensile strength values are higher than those of the commercial alloys Inconel 617 and Alloy 800H, and other compositionally complex alloys (high-entropy alloys).

REFERENCES

1. J.W. Yeh, S.K. Chen, S.J. Lin, J.Y. Gan, T.S. Chin, T.T. Shun, C.H. Tsau, and S.Y. Chang, *Adv. Eng. Mater.* 6, 299 (2004).
2. J.W. Yeh, Y.L. Chen, S.J. Lin, and S.K. Chen, *Mater. Sci. Forum* 560, 1 (2007).
3. A. Manzoni, H. Daoud, S. Mondal, S. van Smaalen, R. Völkl, S. Mondal, U. Glatzel, and N. Wanderka, *J. Alloy. Compd.* 552, 430 (2013).
4. M.C. Gao and D.E. Alman, *Entropy* 15, 4504 (2003).
5. Y. Zhang, T.T. Zuo, Z. Tang, M.C. Gao, K.A. Dahmen, P.K. Liaw, and Z.P. Lu, *Prog. Mater. Sci.* 61, 1 (2014).
6. A.C. Yeh, Y.J. Chang, C.W. Tsai, Y.C. Wang, J.W. Yeh, and C.M. Kuo, *Metall. Mater. Trans. A* 45, 184 (2014).
7. F. Otto, A. Dlouhy, Ch Somsen, H. Bei, G. Eggeler, and E.P. George, *Acta Mater.* 6, 5743 (2013).
8. O.N. Senkov, G.B. Wilks, J.M. Scott, and D.B. Miracle, *Intermetallics* 19, 698 (2011).
9. O.N. Senkov, J.M. Scott, S.V. Senkova, D.B. Miracle, and C.F. Woodward, *J. Alloy. Compd.* 509, 6043 (2011).
10. H.M. Daoud, A. Manzoni, R. Völkl, N. Wanderka, and U. Glatzel, *JOM* 65, 1805 (2013).
11. A. Sengupta, S.K. Putatunda, L. Bartosiewicz, J. Hangas, P.J. Nailos, M. Peputapeck, and F.E. Alberts, *J. Mater. Eng. Perform.* 3, 664 (1994).
12. L. Müller, U. Glatzel, and M. Feller-Kniepmeier, *Acta Metall. Mater.* 41, 3401 (1993).
13. H.M. Daoud, Ph.D. Thesis, Mikrostruktur (2014).
14. K.B. Zhang, Z.Y. Fua, J.Y. Zhang, W.M. Wang, H. Wang, Q.J. Zhang, J. Shi, and J.Y. Zhang, *Mater. Sci. Eng. A* 508, 214 (2009).
15. The Version TCCR, ThermoCalc Software AB, Stockholm, Sweden, 2006. http://www.thermocalc.com.
16. Thermotech Ni-based Superalloys Database, TTNI7, Version 7.0 (Thermo-Calc Software AB, Stockholm, 2006).
17. DIN Deutsches Institut für Normung e.v. (Hrsg.), *DIN-Taschenbuch 205, Materialprüfnormen für metallische Werkstoffe 3-Mechanische-technologische Prüfverfahren (rzeugnisformabhängig), Schweißverbindungen, Metallklebungen*, 3rd ed. (Beuth Verlag, Berlin, 1996), p. 44.
18. C.J. Tong, Y.L. Chen, S.K. Chen, J.W. Yeh, T.T. Shun, C.H. Tsau, S.J. Lin, and S.Y. Chang, *Metall. Mater. Trans. A* 36, 881 (2005).
19. Special Metals Company. http://www.specialmetals.com/documents/Inconel%20alloy%20617.pdf.
20. Sandmeyer Steel Company. http://www.sandmeyersteel.com/images/Alloy800H-800HT-APR2013.pdf.
21. A.V. Kuznetsov, D.G. Shaysultnov, N.D. Stepanov, G.A. Salishchev, and O.N. Senkov, *Mater. Sci. Eng. A* 533, 107 (2012).